ORCA – Online Research @ Cardiff

Equivalent layered models for functionally graded plates

D. Kennedy*, R.K.H. Cheng, S. Wei and F.J. Alcazar Arevalo

Cardiff School of Engineering, Cardiff University, Queen's Buildings, The Parade, Cardiff CF24 3AA, United Kingdom

*Corresponding author. Email kennedyd@cf.ac.uk

Abstract

Functionally graded plates whose material properties vary continuously through the thickness are modelled as exactly equivalent plates composed of up to four isotropic layers. Separate models are derived for analysis using classical plate theory, first-order and higher-order shear deformation theory. For cases where Poisson's ratio varies through the thickness, the integrations required to obtain the membrane, coupling and out-of-plane stiffness matrices are performed accurately using a series solution. The model is verified by comparison with well converged solutions from approximate models in which the plate is divided into many isotropic layers. Critical buckling loads and undamped natural frequencies are found for a range of illustrative examples.

Keywords: functionally graded, plates, vibration, dynamic stiffness, Wittrick-Williams algorithm, transverse shear

1 Introduction

Functionally graded (FG) materials can be defined as those which are formed by gradually mixing two or more different materials, with the main aim of adapting their physical properties to the external environment. The variation of properties is required to be as smooth as possible in order to avoid phenomena such as stress concentrations which could lead to the development or propagation of fractures.

Nature provides examples of materials whose physical properties vary gradually, but the concept of synthetically manufactured FG materials was first developed in Japan in the early 1980s [1]. The simplest kind of FG material is made from gradually varying proportions of two constituent materials, usually with complementary properties. For example, in a FG material composed of metal and a ceramic reinforcement, the ceramic material contributes heat and oxidation resistance, while the metal provides toughness, strength and the bonding capability

needed in order to minimize residual stresses. Furthermore some crucial properties, such as thermal insulation and impact resistance, can be conveyed to the material by varying the internal pore distribution.

Pioneering manufacturing techniques include powder metallurgy, physical and chemical vapour deposition, plasma spraying, self-propagating high temperature synthesis and galvanoforming [1]. Property changes during FG material processing are commonly performed by functions of the chemical composition, microstructure or atomic order, which depend on the position within the element [2]. Property variation through the thickness of a FG plate is achieved by bulk processing or stacking, layer processing by molecular or mechanical deposition, thermal and electrical preform processing or melt processing. It is also possible to vary properties in the same plane by means of technologies such as ultraviolet irradiation [3]. Jet solidification and laser cladding permit greater variation and are suitable for a wide range of layer thicknesses. Solid freeform fabrication is an advanced production technique which can be controlled by computers.

Although the most important applications of FG materials have taken place in the aerospace industry, mechanical engineering, chemical plants and nuclear energy, they are now attracting attention in optics, sports goods, car components, and particularly in biomaterials by means of prostheses. Modern FG implants allow the bone tissues to penetrate between the metallic (often titanium) part and the bone by means of the hydroxyapatite (a transition porous material), forming a graded layup in which a suitable bonding is developed [1].

In engineering it is important to highlight the effects of FG materials in turbomachinery components such as rotating blades, since by varying the gradation it is possible to alter the natural frequencies in order to guarantee stability at particular spinning speeds. Finally it is worth mentioning smart applications, in which piezoelectric sensors and actuators are integrated into the FG material to control vibrations or static responses in structures [3].

Natural frequencies and critical buckling loads of FG plates have been tabulated by various authors [4-7], and it was shown by Abrate [8, 9] that these results are proportional to those for homogeneous isotropic plates. Coupling between in-plane and out-of-plane behaviour can be accounted for by an appropriate choice of the neutral surface [10-12]. Thus the behaviour of FG plates can be predicted from that of similar homogeneous plates. These ideas were exploited to obtain an equivalent isotropic model for a FG plate [13] so that it can be analysed using existing methods based on classical plate theory (CPT) for homogeneous plates. This model was shown to give an exact equivalence when the two component materials have the same Poisson's ratio, but otherwise a small approximation is introduced. The analysis of FG plates with varying Poisson's ratio poses a greater challenge due to the complexity of the integrals which have to be evaluated in order to obtain the in-plane, coupling and flexural stiffness matrices, even when the analysis is restricted to CPT. Efraim proposed an alternative approach [14] in which these integrations are approximated, while the present authors performed the inegrations accurately [15] using a series solution proposed by Dung and Hoa [16].

The present paper includes the previously derived CPT models and examples [13, 15] and then makes important extensions to first-order (FSDT) and higher-order

(HSDT) shear deformation theory so as to permit accurate solutions for thick functionally graded plates. Section 2 introduces an equivalent (single layer) isotropic plate model for use with CPT under the assumption that Poisson's ratio does not vary through the thickness of the plate. This assumption is relaxed in Section 3, where an exactly equivalent plate composed of two isotropic layers is derived for CPT by solving an inverse problem to satisfy six independent stiffness requirements. Section 4 demonstrates that the extension of these models to FSDT is trivial, and then outlines extensions to HSDT giving equivalent plates with three and four layers, respectively. The numerical results in Section 5 verify the proposed models, and also demonstrate its accuracy in finding critical buckling loads and natural frequencies of FG plates, using the different plate theories. Section 6 summarises the conclusions and suggests further extensions to the method.

2 Equivalent isotropic plate for CPT with constant Poisson's ratio

Consider a FG plate of thickness h lying in the xy plane with the origin at mid-surface, having material properties which vary through the thickness (z) direction. Using standard notation, the plate constitutive relations of CPT are written as

$$\mathbf{N} = \mathbf{A}\boldsymbol{\varepsilon}_0 + \mathbf{B}\boldsymbol{\kappa} \qquad\qquad \mathbf{M} = \mathbf{B}\boldsymbol{\varepsilon}_0 + \mathbf{D}\boldsymbol{\kappa} \qquad (1)$$

where the vectors $\mathbf{N}$, $\mathbf{M}$, $\boldsymbol{\varepsilon}_0$ and $\boldsymbol{\kappa}$ contain perturbation membrane forces per unit length, perturbation bending and twisting moments per unit length, perturbation mid-surface membrane strains, and perturbation curvatures and twist, respectively. The membrane, coupling and out-of-plane stiffness matrices are given by

$$\mathbf{A} = \int_{-h/2}^{h/2} E(z)\mathbf{Q}(z)dz \quad \mathbf{B} = \int_{-h/2}^{h/2} E(z)\mathbf{Q}(z)zdz \quad \mathbf{D} = \int_{-h/2}^{h/2} E(z)\mathbf{Q}(z)z^2dz \quad (2)$$

respectively, where

$$\mathbf{Q}(z) = \begin{bmatrix} Q_{11}(z) & Q_{12}(z) & 0 \\ Q_{12}(z) & Q_{11}(z) & 0 \\ 0 & 0 & Q_{66}(z) \end{bmatrix} \qquad (3)$$

with

$$\left. \begin{aligned} Q_{11}(z) &= \frac{1}{1-v(z)^2} \qquad Q_{12}(z) = v(z)Q_{11}(z) \\ Q_{66}(z) &= \frac{1}{2}\big(Q_{11}(z) - Q_{12}(z)\big) \end{aligned} \right\} \qquad (4)$$

3

Young's modulus $E(z)$, Poisson's ratio $v(z)$ and density $\rho(z)$ are assumed to vary through the thickness according to the rule of mixtures

$$E(z) = E_m + V(z)E_\delta \qquad v(z) = v_m + V(z)v_\delta \qquad \rho(z) = \rho_m + V(z)\rho_\delta \qquad (5)$$

where

$$E_\delta = E_r - E_m \qquad v_\delta = v_r - v_m \qquad \rho_\delta = \rho_r - \rho_m \qquad (6)$$

Here, subscripts m and r denote the properties of the metal and reinforcement components, respectively, and $V(z)$ is a function representing the volume fraction of the reinforcement, which is assumed to follow the commonly encountered power law

$$V(z) = \left(\frac{1}{2} + \frac{z}{h}\right)^n \qquad (7)$$

The non-negative volume fraction index n controls the variation of the properties of the FG plate, as illustrated in Figure 1. As n approaches zero the plate consists essentially of reinforcement material, while as n approaches infinity it consists essentially of matrix material.

If both materials have the same Poisson's ratio $v_m = v_r = v_0$, then

$$\mathbf{A} = A_F \mathbf{Q}_0 \qquad \mathbf{B} = B_F \mathbf{Q}_0 \qquad \mathbf{D} = D_F \mathbf{Q}_0 \qquad (8)$$
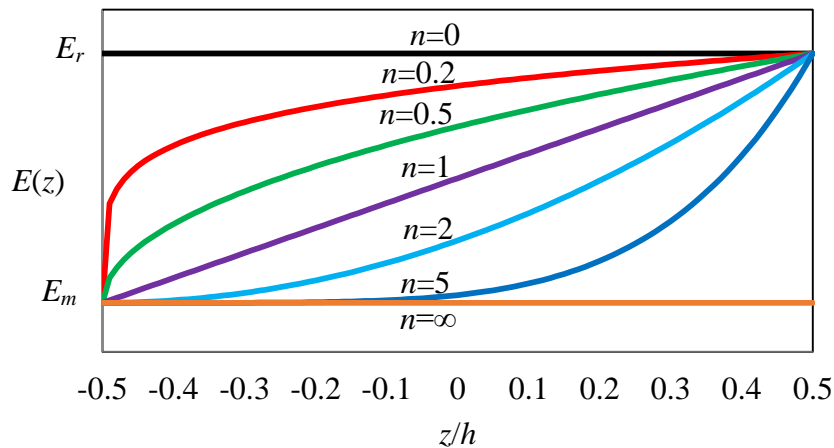
where

Figure 1. Variation of Young's modulus through the thickness of a FG plate with volume fraction index n

$$\mathbf{Q}(z) \equiv \mathbf{Q}_0 = \frac{1}{1 - v_0{}^2} \begin{bmatrix} 1 & v_0 & 0 \\ v_0 & 1 & 0 \\ 0 & 0 & \frac{1}{2}(1 - v_0) \end{bmatrix} \tag{9}$$

and

$$
\left.
\begin{aligned}
A_F &= \int_{-h/2}^{h/2} E(z)dz = h\left(E_m + \frac{E_\delta}{n+1}\right) \\
B_F &= \int_{-h/2}^{h/2} E(z)z\,dz = \frac{h^2}{2}\frac{nE_\delta}{(n+1)(n+2)} \\
D_F &= \int_{-h/2}^{h/2} E(z)z^2 dz = \frac{h^3}{12}\left[E_m + \frac{3(n^2+n+2)E_\delta}{(n+1)(n+2)(n+3)}\right]
\end{aligned}
\right\} \tag{10}
$$

The presence of B_F indicates coupling between the in-plane and out-of-plane behaviour.

Now consider an isotropic plate of thickness h^*, Young's modulus E^*, Poisson's ratio $v^* = v_0$, whose neutral surface is offset by δ^* above the geometric mid-surface. The membrane, coupling and out-of-plane stiffness matrices are given by

$$\mathbf{A} = E^* h^* \mathbf{Q}_0 \qquad \mathbf{B} = E^* h^* \delta^* \mathbf{Q}_0 \qquad \mathbf{D} = E^*\left(\frac{h^{*3}}{12} + h^* \delta^{*2}\right)\mathbf{Q}_0 \tag{11}$$

and is therefore equivalent to the FG plate of Equation (8) if

$$\delta^* = \frac{B_F}{A_F} \qquad h^* = \sqrt{12\left(\frac{D_F}{A_F} - \frac{B_F{}^2}{A_F{}^2}\right)} \qquad E^* = \frac{A_F}{h^*} \tag{12}$$

For vibration analysis an equivalent density ρ^* is also defined, so that the mass per unit area $\rho^* h^*$ of the equivalent plate is equal to that of the FG plate, i.e.

$$\rho^* = \left(\frac{h}{h^*}\right)\left(\rho_m + \frac{\rho_\delta}{n+1}\right) \tag{13}$$

Equations (12) and (13) give an exact isotropic equivalence for FG plates with constant Poisson's ratio. For cases where Poisson's ratio varies through the thickness of the plate, an approximate solution was proposed [13] in which the Poisson's ratio for the equivalent isotropic plate took the mean value for the FG plate, i.e.

$$v^* = \left(v_m + \frac{v_\delta}{n+1}\right) \tag{14}$$

5

3 Equivalent two layer plate for CPT with varying Poisson's ratio

3.1 Normalised stiffness matrices for FG plate

When Poisson's ratio varies through the thickness of the FG plate, Equations (2) cannot be simplified to the form of Equations (8), because the integrations become more complicated on account of the terms in $v(z)$ appearing in the denominators of Equation (4). The independent elements of **A**, **B** and **D** must be evaluated as

$$
\left.
\begin{aligned}
A_{11} &= \int_{-h/2}^{h/2} \frac{E(z)}{1 - v(z)^2}\, dz & A_{12} &= \int_{-h/2}^{h/2} \frac{E(z)v(z)}{1 - v(z)^2}\, dz \\[2mm]
B_{11} &= \int_{-h/2}^{h/2} \frac{E(z)}{1 - v(z)^2}\, z\, dz & B_{12} &= \int_{-h/2}^{h/2} \frac{E(z)v(z)}{1 - v(z)^2}\, z\, dz \\[2mm]
D_{11} &= \int_{-h/2}^{h/2} \frac{E(z)}{1 - v(z)^2}\, z^2\, dz & D_{12} &= \int_{-h/2}^{h/2} \frac{E(z)v(z)}{1 - v(z)^2}\, z^2\, dz
\end{aligned}
\right\}
\tag{15}
$$

Note that as a result of Equation (4),

$$
A_{66} = \frac{1}{2}(A_{11} - A_{12}) \quad B_{66} = \frac{1}{2}(B_{11} - B_{12}) \quad D_{66} = \frac{1}{2}(D_{11} - D_{12})
\tag{16}
$$

Writing

$$
\zeta = \frac{1}{2} + \frac{z}{h} \qquad \bar{E}_\delta = \frac{E_\delta}{E_m}
\tag{17}
$$

Equations (15) can be written in non-dimensional form as

$$
\left.
\begin{aligned}
\bar{A}_{11} &= \frac{A_{11}}{E_m h} = I_0 + \bar{E}_\delta I_n \\[3mm]
\bar{A}_{12} &= \frac{A_{12}}{E_m h} = v_m I_0 + (v_\delta + \bar{E}_\delta v_m)I_n + \bar{E}_\delta v_\delta I_{2n}
\end{aligned}
\right\}
\tag{18}
$$

$$
\left.
\begin{aligned}
\bar{B}_{11} &= \frac{2B_{11}}{E_m h^2} = (2I_1 - I_0) + \bar{E}_\delta(2I_{n+1} - I_n) \\[3mm]
\bar{B}_{12} &= \frac{2B_{12}}{E_m h^2} = \; v_m(2I_1 - I_0) + (v_\delta + \bar{E}_\delta v_m)(2I_{n+1} - I_n) \\
& \qquad\qquad\quad + \bar{E}_\delta v_\delta(2I_{2n+1} - I_{2n})
\end{aligned}
\right\}
\tag{19}
$$

$$
\begin{aligned}
\bar{D}_{11} = \frac{12D_{11}}{E_m h^3} &= (12I_2 - 12I_1 + 3I_0) + \bar{E}_\delta(12I_{n+2} - 12I_{n+1} + 3I_n) \\
\bar{D}_{12} = \frac{12D_{12}}{E_m h^3} &= \quad \nu_m(12I_2 - 12I_1 + 3I_0) \\
&\quad + (\nu_\delta + \bar{E}_\delta \nu_m)(12I_{n+2} - 12I_{n+1} + 3I_n) \\
&\quad + \bar{E}_\delta \nu_\delta(12I_{2n+2} - 12I_{2n+1} + 3I_{2n})
\end{aligned}
\right\} \tag{20}
$$

where the integrals

$$
I_k = \int_0^1 \frac{\zeta^k}{1 - (\nu_m + \nu_\delta \zeta^n)^2} \, d\zeta \tag{21}
$$

are evaluated by means of the series solution [16]

$$
I_k = \frac{1}{2} \sum_{r=0}^{\infty} \frac{c_r}{k + rn + 1} \tag{22}
$$

with

$$
c_r = \left[\frac{1}{(1 - \nu_m)^{r+1}} + \frac{(-1)^r}{(1 + \nu_m)^{r+1}} \right] \nu_\delta^r \tag{23}
$$

3.2 Normalised stiffness matrices for two layer plate

Consider the plate shown in Figure 2, which is made from two layers of different isotropic materials. The figure shows the thicknesses (h_1, h_2), Young's moduli (E_1, E_2) and Poisson's ratios (ν_1, ν_2) of the two layers. The thicknesses and Young's moduli can be expressed in non-dimensional form as

$$
h_1 = \eta_1 h \qquad h_2 = \eta_2 h \qquad E_1 = e_1 E_m \qquad E_2 = e_2 E_m \tag{24}
$$

Application of Equation (2) gives the independent elements of the stiffness matrices **A**, **B** and **D** in non-dimensional form as
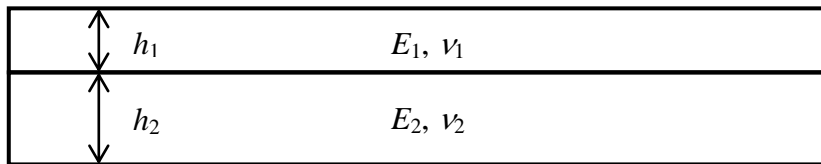

Figure 2: Equivalent two layer plate.

$$\bar{A}_{11}^* = \frac{A_{11}}{E_m h} = K_1 + K_2 \qquad \bar{A}_{12}^* = \frac{A_{12}}{E_m h} = v_1 K_1 + v_2 K_2$$

$$\bar{B}_{11}^* = \frac{2B_{11}}{E_m h^2} = L_1 + L_2 \qquad \bar{B}_{12}^* = \frac{2B_{12}}{E_m h^2} = v_1 L_1 + v_2 L_2 \qquad \qquad (25)$$

$$\bar{D}_{11}^* = \frac{12D_{11}}{E_m h^3} = M_1 + M_2 \quad \bar{D}_{12}^* = \frac{12D_{12}}{E_m h^3} = v_1 M_1 + v_2 M_2$$

where

$$K_1 = \frac{e_1 \eta_1}{1 - v_1^2} \qquad\qquad K_2 = \frac{e_2 \eta_2}{1 - v_2^2} \qquad\qquad (26)$$

$$\qquad\qquad\qquad\qquad\qquad\qquad\qquad\qquad\qquad (27)$$

$$L_1 = -K_1 \eta_2 \qquad\qquad L_2 = K_2 \eta_1$$

$$\qquad\qquad\qquad\qquad\qquad\qquad\qquad\qquad\qquad (28)$$

$$M_1 = K_1(\eta_1^2 + 3\eta_2^2) \qquad M_2 = K_2(3\eta_1^2 + \eta_2^2)$$

3.3 Equivalence of FG plate and two layer plate

Suppose that the non-dimensional stiffnesses of a FG plate and the two layer plate of Section 3.2 have been calculated by Equations (18)-(20) and (25), respectively. Then, for analysis using CPT, the two plates are exactly equivalent if

$$[\bar{A}_{11}^* \quad \bar{A}_{12}^* \quad \bar{B}_{11}^* \quad \bar{B}_{12}^* \quad \bar{D}_{11}^* \quad \bar{D}_{12}^*]^T = [\bar{A}_{11} \quad \bar{A}_{12} \quad \bar{B}_{11} \quad \bar{B}_{12} \quad \bar{D}_{11} \quad \bar{D}_{12}]^T \quad (29)$$

i.e. if

$$K_1 = \frac{-\alpha_2}{v_1 - v_2} \qquad\qquad K_2 = \frac{\alpha_1}{v_1 - v_2} \qquad\qquad (30)$$

$$L_1 = \frac{-\beta_2}{v_1 - v_2} \qquad\qquad L_2 = \frac{\beta_1}{v_1 - v_2} \qquad\qquad (31)$$

$$M_1 = \frac{-\delta_2}{v_1 - v_2} \qquad\qquad M_2 = \frac{\delta_1}{v_1 - v_2} \qquad\qquad (32)$$

where

$$\alpha_1 = v_1 \bar{A}_{11} - \bar{A}_{12} \qquad \alpha_2 = v_2 \bar{A}_{11} - \bar{A}_{12} \qquad\qquad (33)$$

$$\beta_1 = v_1 \bar{B}_{11} - \bar{B}_{12} \qquad \beta_2 = v_2 \bar{B}_{11} - \bar{B}_{12} \qquad\qquad (34)$$

$$\delta_1 = v_1 \bar{D}_{11} - \bar{D}_{12} \qquad \delta_2 = v_2 \bar{D}_{11} - \bar{D}_{12} \qquad\qquad (35)$$

Thus from Equations (33)

$$\nu_1 = \frac{\alpha_1 + \bar{A}_{12}}{\bar{A}_{11}} \qquad\qquad \nu_2 = \frac{\alpha_2 + \bar{A}_{12}}{\bar{A}_{11}} \qquad\qquad (36)$$

and in Equations (34) and (35)

$$\beta_1 = \frac{(\alpha_1 + \bar{A}_{12})\bar{B}_{11}}{\bar{A}_{11}} - \bar{B}_{12} \qquad \beta_2 = \frac{(\alpha_2 + \bar{A}_{12})\bar{B}_{11}}{\bar{A}_{11}} - \bar{B}_{12} \qquad (37)$$

$$\delta_1 = \frac{(\alpha_1 + \bar{A}_{12})\bar{D}_{11}}{\bar{A}_{11}} - \bar{D}_{12} \qquad \delta_2 = \frac{(\alpha_2 + \bar{A}_{12})\bar{D}_{11}}{\bar{A}_{11}} - \bar{D}_{12} \qquad (38)$$

Then, from Equations (27), (30), (31) and (37),

$$\eta_1 = \frac{L_2}{K_2} = \frac{\beta_1}{\alpha_1} = b_1 - b_2\xi_1 \qquad\qquad \eta_2 = -\frac{L_1}{K_1} = -\frac{\beta_2}{\alpha_2} = -b_1 + b_2\xi_2 \qquad (39)$$

where

$$\xi_1 = \frac{1}{\alpha_1} \qquad \xi_2 = \frac{1}{\alpha_2} \qquad b_1 = \frac{\bar{B}_{11}}{\bar{A}_{11}} \qquad b_2 = \bar{B}_{12} - \frac{\bar{A}_{12}\bar{B}_{11}}{\bar{A}_{11}} \qquad (40)$$

Also, from Equations (28), (30), (32) and (38),

$$\frac{M_1}{K_1} = \frac{\delta_2}{\alpha_2} = \eta_1^2 + 3\eta_2^2 = d_1 - \frac{d_2(b_1 + \eta_2)}{b_2} \qquad (41)$$

$$\frac{M_2}{K_2} = \frac{\delta_1}{\alpha_1} = 3\eta_1^2 + \eta_2^2 = d_1 - \frac{d_2(b_1 - \eta_1)}{b_2} \qquad (42)$$

where

$$d_1 = \frac{\bar{D}_{11}}{\bar{A}_{11}} \qquad\qquad d_2 = \bar{D}_{12} - \frac{\bar{A}_{12}\bar{D}_{11}}{\bar{A}_{11}} \qquad (43)$$

Taking the difference between the simultaneous Equations (41) and (42),

$$2(\eta_2^2 - \eta_1^2) = -\frac{d_2(\eta_1 + \eta_2)}{b_2} \qquad (44)$$

which, since the total thickness of the equivalent plate $(\eta_1 + \eta_2)h$ cannot equal zero, implies that

$$\eta_2 = \eta_1 - \frac{d_2}{2b_2} \tag{45}$$

Substituting Equation (45) into the sum of Equations (41) and (42) gives

$$8\eta_1^2 - 4\frac{d_2}{b_2}\eta_1 + \left(\frac{d_2^2}{2b_2^2} - \frac{2(d_1b_2 - d_2b_1)}{b_2}\right) = 0 \tag{46}$$

Solving Equation (46), using Equation (45) and ignoring negative roots,

$$\eta_1 = \left(u + \sqrt{v}\right) \qquad \eta_2 = \left(-u + \sqrt{v}\right) \tag{47}$$

where

$$u = \frac{d_2}{4b_2} \qquad\qquad v = \frac{(d_1b_2 - d_2b_1)}{4b_2} \tag{48}$$

The thicknesses of the two layers are now obtained from Equation (24) as

$$h_1 = \eta_1 h \qquad\qquad h_2 = \eta_2 h \tag{49}$$

The Poisson's ratios are obtained from Equations (36), (39) and (40) as

$$\nu_1 = \frac{1}{\bar{A}_{11}}\left(\frac{b_2}{b_1 - \eta_1} + \bar{A}_{12}\right) \qquad \nu_2 = \frac{1}{\bar{A}_{11}}\left(\frac{b_2}{b_1 + \eta_2} + \bar{A}_{12}\right) \tag{50}$$

Finally, the Young's moduli are found from Equations (24), (26) and (30) as

$$E_1 = \frac{b_2(1 - \nu_1^2)}{\eta_1(\eta_2 + b_1)(\nu_2 - \nu_1)}E_m \qquad E_2 = \frac{b_2(1 - \nu_2^2)}{\eta_2(\eta_1 - b_1)(\nu_2 - \nu_1)}E_m \tag{51}$$

For vibration analysis an equivalent density ρ^* is defined, analogously to that of Equation (13), such that the mass per unit area $\rho^*(h_1 + h_2)$ of the equivalent plate is equal to that of the FG plate, i.e.

$$\rho^* = \left(\frac{1}{\eta_1 + \eta_2}\right)\left(\rho_m + \frac{\rho_\delta}{n + 1}\right) \tag{52}$$

4 Extensions to shear deformation plate theories

4.1 First order shear deformation theory

First order (FSDT) and higher order (HSDT) shear deformation plate theories require the satisfaction of additional constitutive relations beyond those of Equation

(1), and the use of additional stiffness coefficients beyond those listed in Equation (2). In the case of FSDT, Equation (1) is supplemented by the constitutive relation

$$\mathbf{T} = \mathbf{A^s \gamma} \tag{53}$$

between the transverse shear stresses $\mathbf{T}$ and transverse shear strains $\mathbf{\gamma}$. Because the two components of the FG plate are isotropic, the additional stiffness coefficients of $\mathbf{A^s}$ are obtained easily as

$$A_{44} = A_{55} = f A_{66} \qquad A_{45} = 0 \tag{54}$$

where f is the shear correction factor. Thus no additional integrations are required beyond those already used to obtain A_{11} and A_{12} under the assumptions of CPT.

4.2 Higher order shear deformation theory

In the case of HSDT, Equation (1) is replaced by the constitutive relations [17, 18]

$$\begin{bmatrix} \mathbf{N} \\ \mathbf{M} \\ \mathbf{M^*} \end{bmatrix} = \begin{bmatrix} \mathbf{A} & \mathbf{B} & \mathbf{E} \\ \mathbf{B} & \mathbf{D} & \mathbf{F} \\ \mathbf{E} & \mathbf{F} & \mathbf{H} \end{bmatrix} \begin{bmatrix} \mathbf{\epsilon_0} \\ \mathbf{\kappa} \\ \mathbf{\kappa^*} \end{bmatrix} \qquad \begin{bmatrix} \mathbf{T} \\ \mathbf{T^*} \end{bmatrix} = \begin{bmatrix} \mathbf{A^s} & \mathbf{D^s} \\ \mathbf{D^s} & \mathbf{F^s} \end{bmatrix} \begin{bmatrix} \mathbf{\gamma} \\ \mathbf{\gamma^*} \end{bmatrix} \tag{55}$$

where $\mathbf{M^*}$, $\mathbf{\kappa^*}$, $\mathbf{T^*}$ and $\mathbf{\gamma^*}$ denote higher order moments, curvatures, transverse shear stresses and transverse shear strains, respectively. Additional integrations are required to obtain the additional stiffness matrices $\mathbf{E}$, $\mathbf{F}$ and $\mathbf{H}$, while the stiffness coefficients of $\mathbf{D^s}$ and $\mathbf{F^s}$ corresponding to transverse shear effects are obtained as

$$\left. \begin{matrix} D_{44} = D_{55} = D_{66} & D_{45} = 0 \\ F_{44} = F_{55} = F_{66} & F_{45} = 0 \end{matrix} \right\} \tag{56}$$

As a result there are more independent stiffness parameters than those listed in Equations (10) or (15). Therefore an equivalent plate has to comprise more than two layers, as outlined in the following discussion.

To obtain the stiffness matrices of the FG plate, Equation (2) is augmented by

$$\left. \begin{matrix} \mathbf{E} = \int_{-h/2}^{h/2} E(z)\mathbf{Q}(z)z^3 dz \qquad \mathbf{F} = \int_{-h/2}^{h/2} E(z)\mathbf{Q}(z)z^4 dz \\ \mathbf{H} = \int_{-h/2}^{h/2} E(z)\mathbf{Q}(z)z^6 dz \end{matrix} \right\} \tag{57}$$

If Poisson's ratio remains constant through the thickness of the plate, then extension of the arguments of Section 2 leads to

$$\mathbf{E} = E_F \mathbf{Q}_0 \qquad\qquad \mathbf{F} = F_F \mathbf{Q}_0 \qquad\qquad \mathbf{H} = H_F \mathbf{Q}_0 \qquad (58)$$

where

$$E_F = \int_{-h/2}^{h/2} E(z)z^3 dz \qquad F_F = \int_{-h/2}^{h/2} E(z)z^4 dz \qquad H_F = \int_{-h/2}^{h/2} E(z)z^6 dz \qquad (59)$$

There are therefore six independent stiffness properties, A_F, B_F, D_F, E_F, F_F and H_F. An equivalent three layer plate, see Figure 3(a), can therefore be found by selecting six parameters, namely the thicknesses (h_1, h_2, h_3) and Young's moduli (E_1, E_2, E_3) of the three layers, so that the six independent stiffness properties of the equivalent plate match A_F, B_F, D_F, E_F, F_F and H_F of the FG plate. Each layer is assumed to have the same Poisson's ratio as the two components of the FG plate.

If Poisson's ratio varies through the thickness of the plate, extension of the arguments of Section 3 leads to twelve independent stiffness properties, namely those of Equation (15) augmented by

$$\left.\begin{array}{ll}
E_{11} = \displaystyle\int_{-h/2}^{h/2} \frac{E(z)}{1-v(z)^2} z^3 dz & E_{12} = \displaystyle\int_{-h/2}^{h/2} \frac{E(z)v(z)}{1-v(z)^2} z^3 dz \\[3mm]
F_{11} = \displaystyle\int_{-h/2}^{h/2} \frac{E(z)}{1-v(z)^2} z^4 dz & F_{12} = \displaystyle\int_{-h/2}^{h/2} \frac{E(z)v(z)}{1-v(z)^2} z^4 dz \\[3mm]
H_{11} = \displaystyle\int_{-h/2}^{h/2} \frac{E(z)}{1-v(z)^2} z^6 dz & H_{12} = \displaystyle\int_{-h/2}^{h/2} \frac{E(z)v(z)}{1-v(z)^2} z^6 dz
\end{array}\right\} \qquad (60)$$

An equivalent four layer plate, see Figure 3(b), can therefore be found by selecting twelve parameters, namely the thicknesses (h_1, h_2, h_3, h_4), Young's moduli (E_1, E_2, E_3, E_4) and Poisson's ratios (v_1, v_2, v_3, v_4) of the four layers, so that the twelve independent stiffness properties of the equivalent plate match those of the FG plate given in Equations (15) and (60).

The problems of selection of the layer parameters for the HSDT analyses of this section are not readily amenable to analytic solution. However, given suitable trial solutions, they can be solved numerically using the MATLAB software [19].
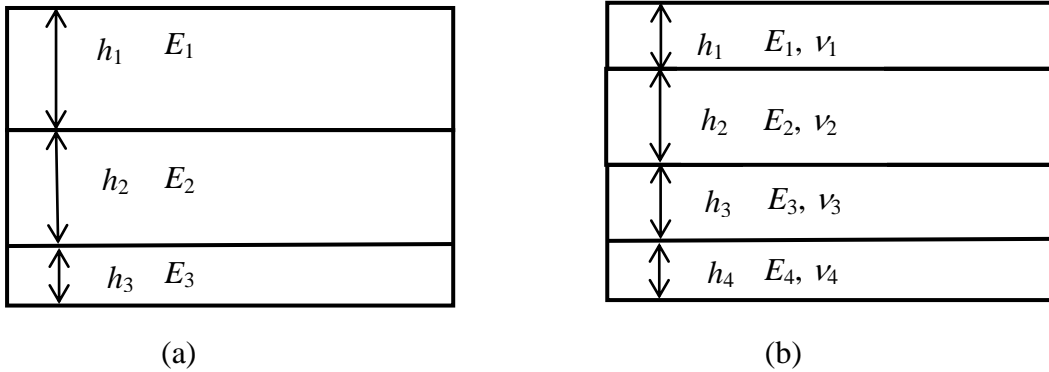

(a) (b)

Figure 3: (a) Equivalent three layer plate; (b) Equivalent four layer plate.

12

Table 1: Summary of equivalent plates for different cases.

Plate theory	Poisson's ratio	No of layers	No of independent stiffness parameters	Independent stiffness parameters	Layer parameters
CPT or FSDT	Constant	1	3	A_F, B_F, D_F	h^*, E^*, δ^*
CPT or FSDT	Varying	2	6	$A_{11}, A_{12}, B_{11}, B_{12},$ D_{11}, D_{12}	$h_1, h_2, E_1, E_2,$ v_1, v_2
HSDT	Constant	3	6	$A_F, B_F, D_F,$ E_F, F_F, H_F	$h_1, h_2, h_3,$ E_1, E_2, E_3
HSDT	Varying	4	12	$A_{11}, A_{12}, B_{11}, B_{12},$ $D_{11}, D_{12}, E_{11}, E_{12},$ $F_{11}, F_{12}, H_{11}, H_{12}$	$h_1, h_2, h_3, h_4,$ $E_1, E_2, E_3, E_4,$ v_1, v_2, v_3, v_4

5 Numerical examples

Table 1 summarises the forms of the equivalent plates for the various cases considered in Sections 2-4. Given any FG plate, the integrations given in these sections enable calculation of the independent stiffness parameters listed in the penultimate column of Table 1. Then solution of between 3 and 12 simultaneous non-linear equations gives the layer parameters listed in the final column of the table, which define an equivalent plate, comprised of between one and four layers and having the same independent stiffness parameters. Hence structural analyses, such as the calculation of critical buckling loads or undamped natural frequencies, can then be performed using existing forms of analysis for plates composed of isotropic layers.

Alternatively, approximate solutions can be obtained by dividing the FG plate into a large number n_l of isotropic layers, each of thickness h/n_l, with the material properties for the ith layer given by Equation (5) with

$$z = \frac{h}{2}\left(-1 + \frac{2i - 1}{n_l}\right) \tag{61}$$

and performing analysis for the resulting laminated plate. Under the assumption that the results from such analysis converge uniformly towards exact results as n_l is increased, a set of results $\{f_{n_l/4}, f_{n_l/2}, f_{n_l}\}$ from the layered model can be used [13] to give an extrapolated prediction

$$\bar{f} = \frac{f_{n_l/4}f_{n_l} - \left(f_{n_l/2}\right)^2}{f_{n_l/4} - 2f_{n_l/2} + f_{n_l}} \tag{62}$$

13

where f_{n_l} represents the result found for the approximate model with n_l layers. Such predictions are taken as comparators for the equivalent isotropic and two layer models presented in this paper.

Such analysis is available in the exact strip software VICONOPT [20], which covers free vibration, critical buckling and postbuckling analysis, and optimum design, of prismatic plate assemblies. In the simplest form of the analysis, which is described in detail in [21], the mode of vibration or buckling is assumed to vary sinusoidally in the prismatic (or longitudinal) direction, giving exact solutions for isotropic and orthotropic stiffened plates and panels in the absence of shear load. Analytical or numerical solution of the governing differential equations in the transverse direction avoids the usual discretisation required by the finite element and finite strip methods. In contrast to finite element analysis, this approach does not involve separate stiffness and mass matrices, but instead yields a transcendental dynamic stiffness matrix which cannot be handled by conventional linear eigensolvers. However the Wittrick-Williams algorithm [22] permits reliable, accurate and rapid convergence on any required eigenvalue, i.e. undamped natural frequency or critical buckling load, and the results which follow represent its first application to FG plates.

5.1 Properties of FG plates with constant Poisson's ratio

The first example considered here is a FG plate of thickness $h = 2$mm, composed of an aluminium matrix reinforced by ceramic material. The aluminium and ceramic have Young's modulus $E_m = 70$GPa and $E_r = 121$GPa, respectively, and both materials have the same Poisson's ratio $\nu_m = \nu_r = \nu_0 = 0.25$. Figure 4 shows plots of the Young's modulus E^*, thickness h^* and neutral surface offset δ^* of the equivalent isotropic plate, obtained using Equations (10) and (12) for different values of the volume fraction index n. Figure 4(a) demonstrates how the equivalent Young's modulus varies from that of the reinforcement material when $n = 0$ to that of the matrix material as n approaches infinity, in agreement with Figure 1 which shows that these represent extreme cases where the FG plate is composed of a single isotopic material.

For these extreme cases, the equivalent isotropic plate is identical to the FG plate. Therefore it has thickness $h^* = h$ and its neutral surface coincides with the geometric mid-surface, i.e. $\delta^* = 0$, as shown in Figures 4(b) and 4(c), respectively. Figure 4(b) shows that the thickness of the equivalent plate can be either larger or smaller than that of the FG plate, by up to about 3% for this example, depending on the value of n. Also, from Figure 4(c), the neutral surface of the equivalent plate is always offset above its geometric mid-surface, by up to 5% of the true thickness h. It can be shown analytically from Equations (10) and (12) that the greatest offset is given by

$$\delta^* = \frac{h}{2} \left[\frac{(E_r - E_m)}{\left(\sqrt{E_r} + \sqrt{2E_m} \right)^2} \right] \tag{63}$$
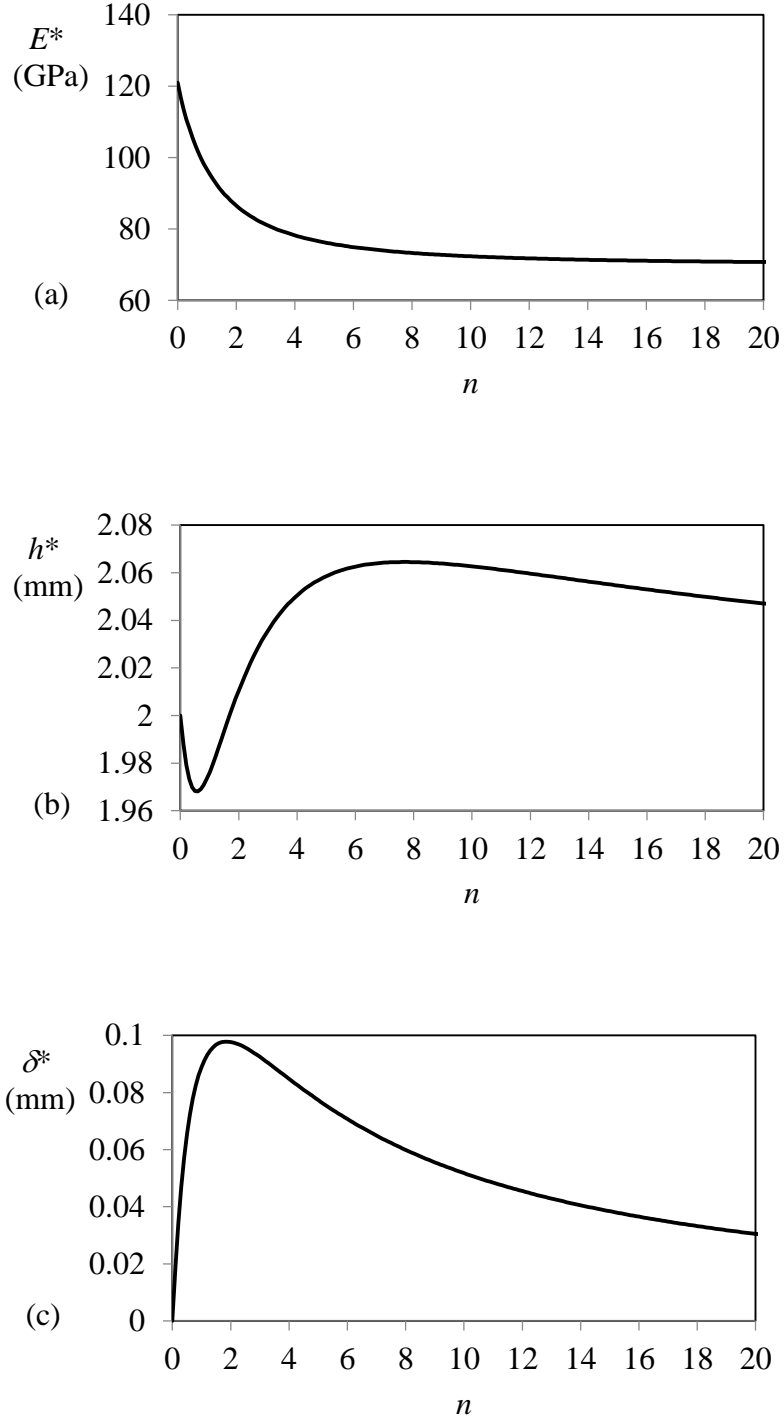
14

Figure 4: Plots of (a) equivalent Young's modulus E^*, (b) equivalent thickness h^*, and (c) neutral surface offset δ^* against volume fraction index n, for an aluminium-ceramic FG plate of thickness $h = 2\text{mm}$

and occurs when $n = \sqrt{2E_r/E_m}$.

Table 2 demonstrates that the stiffness matrices obtained using VICONOPT by the approximate layered approach, with $n_l = 128$ and extrapolated by Equation (62), converge exactly to those of the equivalent isotropic plate. Table 2 also lists the Young's modulus E^*, thickness h^* and neutral surface offset δ^* of the equivalent isotropic plate.

Table 2: Properties of equivalent isotropic plate, and convergence of stiffness matrices for an aluminium-ceramic FG plate.

|	$n = 0.2$	$n=0.5$	$n = 1$	$n = 2$	$n = 5$
Approximate, $n_l = 128$					
A_{11} (Nm^{-1})	240010	221870	203730	185600	167470
A_{12} (Nm^{-1})	60004	55468	50933	46400	41866
B_{11} (N)	8227.4	14501	18132	18132	12950
B_{12} (N)	2056.8	3625.4	4533.1	4533.1	3237.6
D_{11} (Nmm)	78641	72579	67911	64284	60138
D_{12} (Nmm)	19660	18145	16978	16071	15034
Extrapolated, Eq. (62)					
A_{11} (Nm^{-1})	240000	221860	203730	185600	167480
A_{12} (Nm^{-1})	60002	55467	50933	46400	41866
B_{11} (N)	8242.0	14506	18133	18133	12951
B_{12} (N)	2060.4	3626.7	4533.4	4533.1	3238.0
D_{11} (Nmm)	78626	72574	67911	64285	60141
D_{12} (Nmm)	19656	18144	16978	16072	15034
Equivalent isotropic plate [13]					
E^* (GPa)	113.683	105.678	96.655	86.549	76.268
h^* (mm)	1.9792	1.9682	1.9761	2.0104	2.0585
δ^* (mm)	0.0343	0.0654	0.0890	0.0977	0.0773
A_{11} (Nm^{-1})	240000	221870	203730	185600	167470
A_{12} (Nm^{-1})	60000	55467	50933	46400	41867
B_{11} (N)	8242.4	14507	18133	18133	12952
B_{12} (N)	2060.6	3626.7	4533.3	4533.3	3238.1
D_{11} (Nmm)	78626	72574	67911	64284	60140
D_{12} (Nmm)	19657	18143	16978	16071	15035
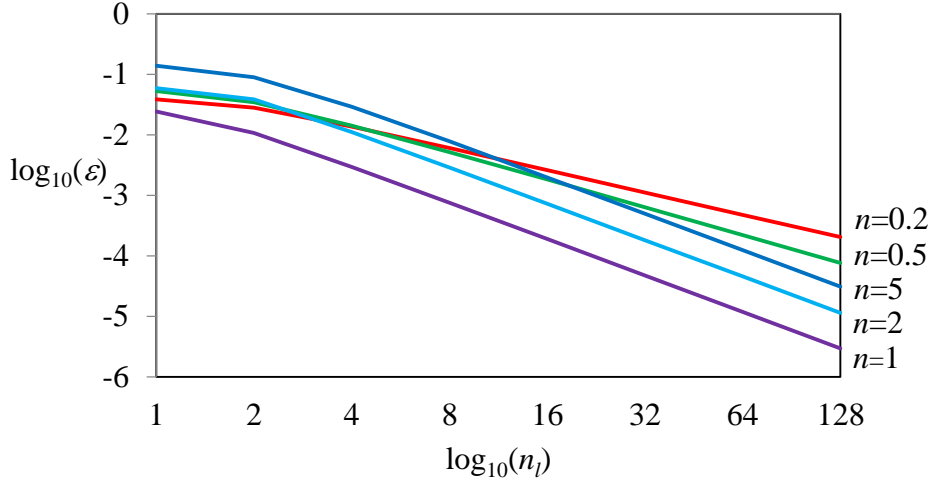
Figure 5: Relative errors in the critical buckling load of a square simply supported aluminium-ceramic FG plate with volume fraction index n, comparing a layered solution with n_l layers and the analytical solution for an equivalent isotropic plate.

5.2 Critical buckling of FG plates with constant Poisson's ratio

A simply supported square aluminium-ceramic FG plate of length $a = 100$mm, thickness $h = 2$mm and the material properties given in Section 5.1 was loaded in uniform longitudinal compression. For seven values of the volume fraction index, ranging from $n = 0$ (i.e. pure ceramic) to $n = \infty$ (i.e. pure metal), the software VICONOPT was used to find the critical buckling load, firstly by using an analytical model of the equivalent isotropic plate defined in Section 2, and secondly by using an approximate layered model with up to $n_l = 128$ isotropic layers. The analytical results can be regarded as exact for this example because both materials have the same Poisson's ratio.

Table 3: Critical buckling load of a square simply supported aluminium-ceramic FG plate with volume fraction index n, comparing the analytical solution for an equivalent isotropic plate, the approximate layered solution with $n_l = 128$ layers, and extrapolations from the layered solutions obtained using Equation (62).

	P_{cr} (kN)			Relative error	
n	Analytical	Approximate	Extrapolated	Approximate	Extrapolated
0	33.96899	33.96899	33.96899	0.00	0.00
0.2	30.92865	30.93497	30.92874	2.04×10^{-4}	2.73×10^{-6}
0.5	28.27660	28.27876	28.27660	7.64×10^{-5}	3.18×10^{-7}
1	26.17307	26.17314	26.17306	2.94×10^{-6}	-5.53×10^{-8}
2	24.67906	24.67878	24.67906	-1.14×10^{-5}	-9.00×10^{-9}
5	23.34671	23.34599	23.34671	-3.10×10^{-5}	-4.71×10^{-9}
∞	19.65148	19.65148	19.65148	0.00	0.00

Table 4: Properties of equivalent isotropic and two layer plates, and convergence of stiffness matrices for a Ti-AlOx FG plate, with $\nu_m = 0.26$ and $\nu_r = 0.2884$.

	$n = 0.2$	$n{=}0.5$	$n = 1$	$n = 2$	$n = 5$
Approximate, $n_l = 128$					
A_{11} (Nm^{-1})	348630	429440	509850	590000	669960
A_{12} (Nm^{-1})	98624	119020	138660	157770	176500
B_{11} (N)	-36816	-64550	-80391	-80138	-57091
B_{12} (N)	-9597.5	-16229	-19632	-19108	-13342
D_{11} (Nmm)	122260	149160	169780	185830	204220
D_{12} (Nmm)	34373	40964	45869	49724	54235
Extrapolated, Eq. (62)					
A_{11} (Nm^{-1})	348690	429470	509850	590000	669950
A_{12} (Nm^{-1})	98638	119030	138660	157770	176490
B_{11} (N)	-36880	-64572	-80396	-80142	-57100
B_{12} (N)	-9612.1	-16233	-19633	-19109	-13344
D_{11} (Nmm)	122310	149180	169780	185830	204210
D_{12} (Nmm)	34389	40964	45869	49723	54232
Equivalent isotropic plate [13]					
E^* (GPa)	158.880	200.884	245.712	290.726	330.279
h^* (mm)	2.0190	1.9735	1.9214	1.8842	1.8876
δ^* (mm)	-0.1072	-0.1527	-0.1603	-0.1381	-0.0867
A_{11} (Nm^{-1})	348850	429890	510490	590660	670420
A_{12} (Nm^{-1})	98958	119910	139980	159160	177480
B_{11} (N)	-37402	-65638	-81815	-81588	-58118
B_{12} (N)	-10610	-18308	-22434	-21985	-15386
D_{11} (Nmm)	122520	149550	170160	186010	204100
D_{12} (Nmm)	34754	41714	46659	50123	54032
Equivalent two layer plate					
E_1 (GPa)	225.542	303.602	346.969	358.940	354.721
ν_1	0.2770	0.2688	0.2638	0.2612	0.2602
h_1 (mm)	0.5868	0.6297	0.7617	0.9951	1.3724
E_2 (GPa)	137.684	156.770	177.391	199.647	225.007
ν_2	0.2869	0.2848	0.2822	0.2789	0.2751
h_2 (mm)	1.3814	1.3093	1.1716	0.9547	0.6072
A_{11} (Nm^{-1})	348690	429460	509850	590000	669960
A_{12} (Nm^{-1})	98639	119030	138660	157770	176500
B_{11} (N)	-36882	-64573	-80396	-80143	-57100
B_{12} (N)	-9612.7	-16234	-19634	-19109	-13344
D_{11} (Nmm)	122330	149180	169780	185830	204210
D_{12} (Nmm)	34388	40969	45869	49722	54233

Table 5: Properties of equivalent isotropic and two layer plates, and convergence of stiffness matrices for a Ti-AlOx FG plate, with $v_m = 0.15$ and $v_r = 0.4$.

	$n = 0.2$	$n=0.5$	$n = 1$	$n = 2$	$n = 5$
Approximate, $n_l = 128$					
A_{11} (Nm^{-1})	366820	438360	508380	577660	646550
A_{12} (Nm^{-1})	129300	132910	131050	125520	117370
B_{11} (N)	-33887	-56991	-70005	-69274	-49162
B_{12} (N)	-4277.7	-2328.7	1850.3	5530.5	6056.5
D_{11} (Nmm)	127480	150910	168820	182900	198990
D_{12} (Nmm)	43063	42637	41165	40346	40100
Extrapolated, Eq. (62)					
A_{11} (Nm^{-1})	366870	438380	508380	577660	646540
A_{12} (Nm^{-1})	129290	132900	131060	125530	117360
B_{11} (N)	-33441	-57011	-70010	-69278	-49171
B_{12} (N)	-4266.1	-2324.0	1850.3	5530.0	6055.1
D_{11} (Nmm)	127550	150940	168820	182900	198980
D_{12} (Nmm)	43055	42631	41164	40345	40099
Equivalent isotropic plate [13]					
E^* (GPa)	158.880	200.884	245.712	290.726	330.279
h^* (mm)	2.0190	1.9735	1.9214	1.8842	1.8876
δ^* (mm)	-0.1072	-0.1527	-0.1603	-0.1381	-0.0867
A_{11} (Nm^{-1})	368040	440630	510730	579310	647210
A_{12} (Nm^{-1})	131880	139530	140450	135170	124050
B_{11} (N)	-39459	-67277	-81854	-80020	-56106
B_{12} (N)	-14140	-21304	-22510	-18671	-10754
D_{11} (Nmm)	129260	153280	170240	182440	197040
D_{12} (Nmm)	46317	48540	46817	42568	37765
Equivalent two layer plate					
E_1 (GPa)	219.628	296.554	339.572	354.349	353.286
v_1	0.3007	0.2292	0.1847	0.1609	0.1515
h_1 (mm)	0.6096	0.6621	0.7957	1.0240	1.3899
E_2 (GPa)	136.901	154.867	174.719	196.802	222.547
v_2	0.3871	0.3695	0.3472	0.3197	0.2864
h_2 (mm)	1.3643	1.2886	1.1509	0.9360	0.5938
A_{11} (Nm^{-1})	366880	438370	508380	577660	646540
A_{12} (Nm^{-1})	129290	132900	131050	125520	117370
B_{11} (N)	-33443	-57010	-70009	-69279	-49170
B_{12} (N)	-4268.9	-2324.1	1850.4	5529.9	6055.1
D_{11} (Nmm)	127530	150920	168820	182890	198980
D_{12} (Nmm)	43054	42632	41164	40346	40098

Figure 5 shows that the results from the layered model converge towards the analytical results as n_l is increased, giving 4 to 6 significant figures of accuracy when $n_l = 128$. Table 3 shows that these extrapolated predictions from Equation (62) are even closer to the analytical results, demonstrating the correctness of the equivalent isotropic model.

5.3 Properties of FG plates with varying Poisson's ratio

Abrate [8] studied the free vibration of FG plates composed of a titanium alloy (Ti) matrix reinforced by aluminium oxide (AlOx). The titanium had Young's modulus $E_m = 349.55$GPa, Poisson's ratio $\nu_m = 0.26$ and density $\rho_m = 3750$kgm^{-3}, while the aluminium oxide had Young's modulus $E_r = 122.56$GPa, Poisson's ratio $\nu_r = 0.2884$ and density $\rho_r = 4429$kgm^{-3}. Table 4 illustrates that the stiffness matrices for such a plate with thickness $h = 2$mm, obtained by VICONOPT using the approximate layered approach with $n_l = 128$ and extrapolated by Equation (62), converge to those of the equivalent two layer plate proposed in this paper, rather than to those of the previously proposed isotropic plate [13]. The reason for the superior accuracy of the two layer model is that it accounts exactly for the variation in Poisson's ratio, in contrast to the approximation introduced by Equation (14) for the isotropic plate. This accuracy is confirmed by Table 5, where the Poisson's ratios of the component materials have been artificially adjusted to give a more extreme variation between them, namely $\nu_m = 0.15$ and $\nu_r = 0.4$.

5.4 Natural frequencies of FG plates with varying Poisson's ratio

The software VICONOPT was used to find the fundamental natural frequencies of simply supported square FG plates of length $a = 100$mm with the composition described in Section 5.3, for seven values of the volume fraction index, ranging from $n = 0$ (i.e. pure reinforcement) to $n = \infty$ (i.e. pure matrix). As in Section 5.2, results from an analytical model of the equivalent isotropic plate were compared with those from an approximate layered model with up to $n_l = 128$ isotropic layers, and with extrapolated predictions from the latter. Figure 6 shows agreement to approximately 4 significant figures between the analytical and approximate results.

However, in contrast to the example of Section 5.2, Table 6 shows that this accuracy cannot be significantly improved by extrapolation, indicating that as n_l is increased the layered model converges to natural frequencies which differ slightly from those of the equivalent isotropic plate. The reason for this is the approximation introduced by Equation (14) to obtain a constant value of Poisson's ratio for the equivalent isotropic model.

The natural frequencies ω_{ij} of a simply supported square isotropic plate of length a and thickness h, with Young's modulus E, Poisson's ratio ν and density ρ, are given by the expression [23]
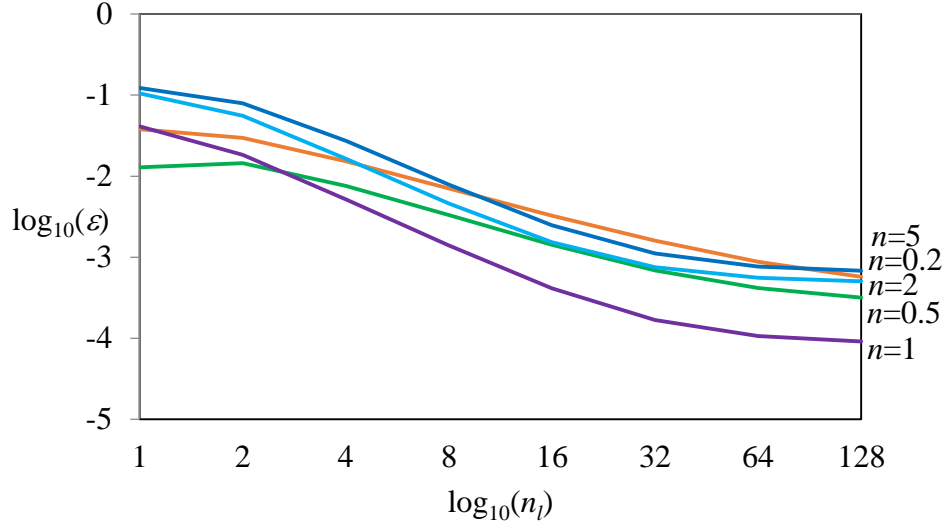
20

Figure 6: Relative errors in the fundamental natural frequency of a square simply supported AlOx-Ti FG plate with $v_m = 0.26$, $v_r = 0.2884$ and volume fraction index n, comparing a layered solution with n_l layers and the analytical solution for an equivalent isotropic plate.

$$\omega_{ij} = \frac{\pi h}{4a^2} \left[\sqrt{\frac{E}{3\rho(1-\nu^2)}} \right] (i^2 + j^2) \tag{64}$$

where i and j represent the number of half-waves in the longitudinal and transverse directions, respectively. Hence the natural frequencies can be written in the normalised form

Table 6: Fundamental natural frequency of a square simply supported AlOx-Ti FG plate with volume fraction index n, comparing the analytical solution for an equivalent isotropic plate, the approximate layered solution with $n_l = 128$ layers, and extrapolations from the layered solutions obtained using Equation (62).

n	ω_{11}			Relative error	
	Analytical	Approximate	Extrapolated	Approximate	Extrapolated
0	996.477	996.477	996.477	0.00	0.00
0.2	1163.675	1163.006	1163.274	-5.75×10^{-4}	-3.45×10^{-4}
0.5	1279.568	1279.162	1279.234	-3.17×10^{-4}	-2.61×10^{-4}
1	1376.225	1376.351	1376.343	9.15×10^{-5}	8.63×10^{-5}
2	1472.185	1472.931	1472.907	5.07×10^{-4}	4.90×10^{-4}
5	1594.158	1595.245	1595.199	6.82×10^{-4}	6.53×10^{-4}
∞	1813.540	1813.540	1813.540	0.00	0.00

21

Table 7: Natural frequencies ω_{ij} of a square simply supported AlOx-Ti FG plate with volume fraction index n, normalised with respect to the corresponding fundamental natural frequency ω_{11}.

n	ω_{11}/ω_{11}	ω_{12}/ω_{11}	ω_{22}/ω_{11}	ω_{13}/ω_{11}	ω_{23}/ω_{11}	ω_{14}/ω_{11}
0	1.0000	2.5000	4.0000	5.0000	6.5000	8.5000
0.2	1.0000	2.4987	3.9960	4.9933	6.4881	8.4787
0.5	1.0000	2.4988	3.9962	4.9936	6.4886	8.4797
1	1.0000	2.4989	3.9964	4.9939	6.4892	8.4807
2	1.0000	2.4989	3.9965	4.9942	6.4896	8.4815
5	1.0000	2.4989	3.9965	4.9942	6.4896	8.4814
∞	1.0000	2.5000	4.0000	5.0000	6.5000	8.5000

$$\frac{\omega_{ij}}{\omega_{11}} = \frac{1}{2}(i^2 + j^2) \tag{65}$$

Table 7 shows that this relationship is satisfied exactly for FG plates with extreme values of the volume fraction index $n = 0$ and $n = \infty$. The remaining cases in Table 7 were obtained using the equivalent isotropic model, and show slight discrepancies from the analytical results due to the approximation in the representation of Poisson's ratio by Equation (14). However the discrepancies can be avoided by using the equivalent two layer model rather than the equivalent isotropic model.

5.5 Vibration of thick FG plates with varying Poisson's ratio

VICONOPT was used to find the first three undamped natural frequencies of a thick Ti-AlOx FG plate with the same material properties as the plate of Table 4. The plate had length and width 100mm and thickness $h = 10$mm. Tables 8 and 9 list the results obtained by the approximate layered approach with $n_l = 128$ and extrapolated by Equation (62), and by the equivalent isotropic and two layer plates, using CPT and FSDT (with shear correction factor $\kappa = 5/6$) respectively. Both tables show that the approximate layered results converge to those of the two layer plate, making this an ideal representation of the FG plate whichever theory is chosen. The significant difference between most of the corresponding results in Tables 8 and 9 illustrates the necessity to account for transverse shear deformation in the vibration analysis of moderately thick plates.

VICONOPT is currently unable to carry out buckling or vibration analysis based on HSDT. However the stiffness calculations of Section 4 have been coded and verified by the fourth author in an extensive parametric study [24] which will permit their future use in alternative HSDT software for plates composed of isotropic layers.

Table 8: First three natural frequencies of equivalent isotropic and two layer plates, for a thick Ti-AlOx FG plate with $\nu_m = 0.26$ and $\nu_r = 0.2884$, found by CPT.

	$n = 0.2$	$n=0.5$	$n = 1$	$n = 2$	$n = 5$
Approximate, $n_l = 128$					
ω_1 (Hz)	182.403	200.549	215.754	230.914	250.160
ω_2 (Hz)	450.361	494.899	532.300	569.781	617.549
ω_3 (Hz)	454.184	512.277	567.302	620.259	671.850
Extrapolated, Eq. (62)					
ω_1 (Hz)	182.445	200.562	215.752	230.910	250.152
ω_2 (Hz)	450.440	494.926	532.298	569.771	617.531
ω_3 (Hz)	454.221	512.221	567.302	620.257	671.847
Equivalent isotropic plate [13]					
ω_1 (Hz)	182.531	200.781	216.033	231.160	250.305
ω_2 (Hz)	450.788	496.121	534.124	571.762	619.094
ω_3 (Hz)	454.143	512.095	567.034	619.990	671.664
Equivalent two layer plate					
ω_1 (Hz)	182.495	200.680	215.914	231.067	250.258
ω_2 (Hz)	450.769	495.653	533.273	570.729	618.170
ω_3 (Hz)	454.226	512.286	567.299	620.255	671.845

Table 9: First three natural frequencies of equivalent isotropic and two layer plates, for a thick Ti-AlOx FG plate with $\nu_m = 0.26$ and $\nu_r = 0.2884$, found by FSDT.

	$n = 0.2$	$n=0.5$	$n = 1$	$n = 2$	$n = 5$
Approximate, $n_l = 128$					
ω_1 (Hz)	178.175	196.153	211.131	226.324	245.116
ω_2 (Hz)	426.587	469.174	506.301	544.878	589.039
ω_3 (Hz)	454.122	512.157	567.146	620.130	671.790
Extrapolated, Eq. (62)					
ω_1 (Hz)	178.220	196.167	211.130	226.320	245.110
ω_2 (Hz)	426.706	470.217	506.299	543.869	589.023
ω_3 (Hz)	454.169	512.171	567.146	620.129	671.786
Equivalent isotropic plate [13]					
ω_1 (Hz)	177.762	195.785	210.952	225.953	244.683
ω_2 (Hz)	424.072	468.006	505.387	542.200	587.174
ω_3 (Hz)	454.143	512.095	567.034	619.990	671.664
Equivalent two layer plate					
ω_1 (Hz)	178.004	195.975	211.133	226.173	244.979
ω_2 (Hz)	425.534	469.161	506.289	543.049	588.299
ω_3 (Hz)	454.176	512.189	567.182	620.160	671.804

6 Conclusions and further work

An equivalent two layer model has been developed for a functionally graded (FG) plate whose material properties, including Poisson's ratio, vary continuously through the thickness. The model allows critical buckling loads and undamped natural frequencies of a FG plate to be obtained using existing methods based on classical plate theory (CPT) or first order shear deformation plate theory (FSDT) for plates composed of isotropic layers. Analytic expressions have been derived for the thickness, Young's modulus, Poisson's ratio and density of the component layers. The model gives an exact analogy with the FG plate, so extending and improving a previously proposed isotropic plate model which however remains exact if the matrix and reinforcement materials have the same Poisson's ratio.

The two layer plate model has been verified by using the software VICONOPT to obtain the stiffness properties for a simply supported FG plate. The correctness and accuracy of the model have been confirmed by comparing these results with well converged solutions from an approximate model in which the plate is divided into isotropic layers. Agreement has also been demonstrated in the calculation of undamped natural frequencies, using both CPT and FSDT, for a thick FG plate.

Because the equivalent model can be used directly with established software such as VICONOPT, the analysis is readily extended to FG plates with different loading and support conditions, and to prismatic panels containing such plates, e.g. aircraft wing and fuselage panels. Attention will also be given to FG plates whose volume fraction varies in different ways through the thickness of the plate.

CPT and FSDT give satisfactory results for thin and moderately thick plates, respectively, but should be replaced by a more accurate higher order shear deformation theory when analysing thicker plates of the dimensions used in composite aircraft panels. The methods proposed in this paper have therefore been extended to obtain equivalent plates composed of three and four isotropic layers, which exhibit the additional material properties needed to fully represent the FG material when using higher order theories. Critical buckling and undamped vibration studies for such plates will be perfomed using alternative HSDT software for plates composed of isotropic layers.

References

[1] Y. Miyamoto, W.A. Kaysser, B.H. Rabin, A. Kawasaki, R.G. Ford, "Functionally Graded Materials: Design, Processing and Applications", Kluwer Academic Publishers, Dordrecht, Netherlands, 1999.

[2] B. Kieback, A. Neubrand, H. Riedel, "Processing techniques for functionally graded materials", Materials Science and Engineering: A, 362(1-2), 81–105, 2003.

[3] L.W. Byrd, V. Birman, "Modeling and analysis of functionally graded materials and structures", Applied Mechanics Reviews, 60(1-6), 195-216, 2007.

[4]   K.M. Liew, J. Yang, S. Kitipornchai, "Postbuckling of piezoelectric FGM plates subject to thermo-electro-mechanical loading", International Journal of Solids and Structures, 40(15), 3869-3892, 2003.

[5]   J. Yang, H.-S. Shen, "Dynamic response of initially stressed functionally graded rectangular thin plates", Composite Structures, 54(4), 497-508, 2001.

[6]   X.Q. He, T.Y. Ng, S. Sivashanker, K.M. Liew, "Active control of FGM plates with integrated piezoelectric sensors and actuators", International Journal of Solids and Structures, 38(9), 1641-1655, 2001.

[7]   J. Yang, H.-S. Shen, "Vibration characteristics and transient response of shear-deformable functionally graded plates in thermal environments", Journal of Sound and Vibration, 255(3), 579-602, 2002.

[8]   S. Abrate, "Free vibration, buckling, and static deflections of functionally graded plates", Composites Science and Technology, 66(14), 2382-2394, 2006.

[9]   S. Abrate, "Functionally graded plates behave like homogeneous plates", Composites: Part B, 39(1), 151-158, 2008.

[10]   T. Morimoto, Y. Tanigawa, R. Kawamura, "Thermal buckling of functionally graded rectangular plates subjected to partial heating", International Journal of Mechanical Sciences, 48(9), 926-937, 2006.

[11]   D.G. Zhang, Y.H. Zhou, "A theoretical analysis of FGM thin plates based on physical neutral surface", Computational Materials Science, 44(2), 716-720, 2008.

[12]   T. Prakash, M.K. Singha, M. Ganapathi, "Influence of neutral surface position on the nonlinear stability behavior of functionally graded plates", Computational Mechanics, 43(3), 341-350, 2009.

[13]   D. Kennedy, R.K.H. Cheng, "An equivalent isotropic model for functionally graded plates", in B.H.V. Topping (Editor), "Proceedings of 11th International Conference on Computational Structures Technology", Civil-Comp Press, Stirlingshire, UK, Paper 94, 2012. doi:10.4203/ccp.99.94.

[14]   E. Efraim, "Accurate formula for determination of natural frequencies of FGM plates basing on frequencies of isotropic plates", Procedia Engineering, 10, 242-247, 2011.

[15]   D. Kennedy, S. Wei, F.J. Alcazar Arevalo, "Two layer model of functionally graded plate with varying Poisson's ratio", in B.H.V. Topping, P. Iványi (Editors), "Proceedings of 12th International Conference on Computational Structures Technology", Civil-Comp Press, Stirlingshire, UK, Paper 34, 2014. doi:10.4203/ccp.106.34.

[16]   D.V. Dung, L.K. Hoa, "Nonlinear analysis of buckling and postbuckling for axially compressed functionally graded cylindrical panels with the Poisson's ratio varying smoothly along the thickness", Vietnam Journal of Mechanics, 34(1), 27-44, 2012.

[17]   K.K. Pradhan, S. Chakraverty, "Effects of different shear deformation theories on free vibration of functionally graded beams", International Journal of Mechanical Sciences, 82, 149-160, 2014.

[18]   J.N. Reddy, "Analysis of functionally graded plates", International Journal for Numerical Methods in Engineering, 47(1-3), 663-684, 2000.

[19]   MATLAB version 8.4, release R2014b, The Mathworks, Inc., Natick, MA, USA, 2014.

[20]   D. Kennedy, C.A. Featherston, "Exact strip analysis and optimum design of aerospace structures", Aeronautical Journal, 114(1158), 505-512, 2010.

[21]   W.H. Wittrick, F.W. Williams, "Buckling and vibration of anisotropic or isotropic plate assemblies under combined loadings", International Journal of Mechanical Sciences, 16(4), 209-239, 1974.

[22]   W.H. Wittrick, F.W. Williams, "A general algorithm for computing natural frequencies of elastic structures", Quarterly Journal of Mechanics and Applied Mathematics, 24(3), 263-284, 1971.

[23]   C.F. Beards, "Structural Vibration: Analysis and Damping", Elsevier, Oxford, 1996.

[24]   F.J. Alcazar Arevalo, "Equivalent models of a functionally graded plate based on the classical plate theory and the third order shear deformation theory", MSc thesis, Cardiff University, UK, 2014.